IEEE Photonics Journal
An IEEE Photonics Society Publication

Open Access

Wideband Doppler Frequency Shift Measurement and Direction Discrimination Based on a DPMZM

Volume 9, Number 2, April 2017

Wei Chen
Aijun Wen, *Senior Member, IEEE*
Xiaoyan Li
Yongsheng Gao
Yong Wang
Shuiying Xiang
Hongye He
Hanxiao Zheng

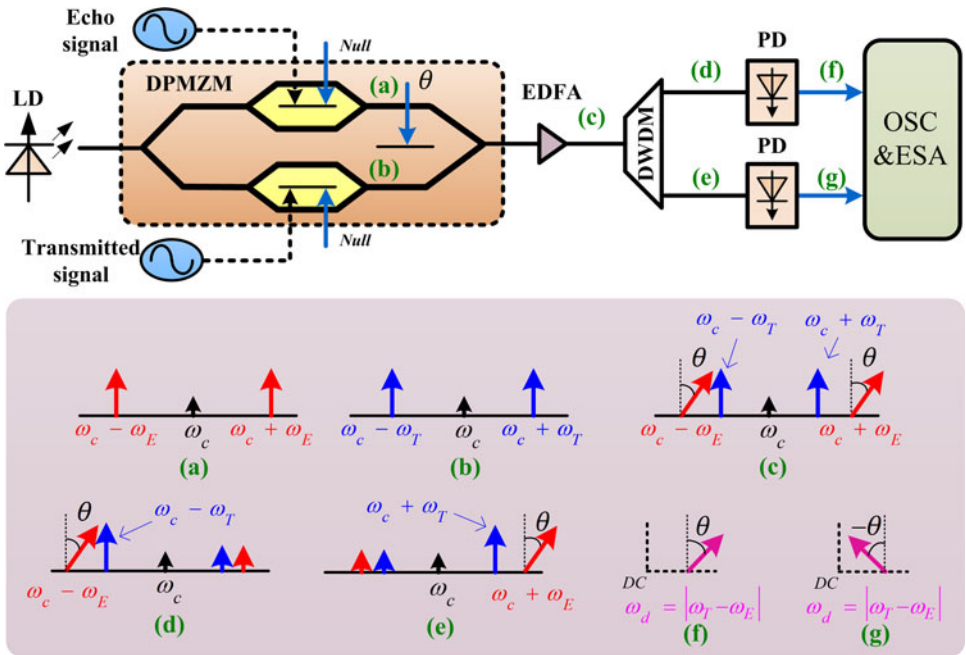

DOI: 10.1109/JPHOT.2017.2676988
1943-0655

Wideband Doppler Frequency Shift Measurement and Direction Discrimination Based on a DPMZM

Wei Chen,[1,2] Aijun Wen,[1,2] *Senior Member, IEEE*, Xiaoyan Li,[1,2] Yongsheng Gao,[1,2] Yong Wang,[1,2] Shuiying Xiang,[1,2] Hongye He,[1,2] and Hanxiao Zheng[1,2]

[1]State Key Laboratory of Integrated Services Networks, Xidian University, Xi'an 710071, China
[2]Collaborative Innovation Center of Information Sensing and Understanding, Xidian University, Xi'an 710071, China

DOI:10.1109/JPHOT.2017.2676988

Manuscript received January 19, 2017; revised February 20, 2017; accepted February 27, 2017. Date of publication March 2, 2017; date of current version March 20, 2017. This work was supported in part by the National Natural Science Foundation of China under Grant 61674119 and in part by the China 111 project under Grant B08038. Corresponding author: A. Wen (ajwen@xidian.edu.cn).

Abstract: A wideband microwave Doppler frequency shift (DFS) measurement approach based on a single dual-parallel Mach–Zehnder modulator (DPMZM) is proposed and experimentally demonstrated. The light wave is modulated by the transmitted and echo signals in the DPMZM to generate carrier suppressed double sidebands signals. Based on the phase difference and powers of the upper bands and lower bands of the modulated signal, the DFS value, as well as the sign, can be measured. An experiment is carried out. The DFS from –100 to +100 kHz at the carrier frequencies of 10, 20, 30, and 39 GHz is accurately measured with errors of less than 5×10^{-6} Hz.

Index Terms: Doppler frequency shift (DFS), microwave photonics, carrier suppressed double sidebands modulation (CS-DSB), wide frequency range

1. Introduction

Microwave photonics has made enormous strides in the last few years [1] and is widely deemed as the alternative technology of the electronic counterpart in many aspects of radio frequency (RF) engineering from radar systems [2], [3], warfare reconnaissance receivers, and wireless communication [4], [5] to aerospace technology [6], thanks to its inherent advantages such as light weight, large bandwidth, low transmission loss, and immunity to electromagnetic interference (EMI). Among these fields, photonic-based microwave measurement technology has become a subject of active research. It suggests the possibility of realizing the RF measurement covering the entire range of frequencies from few megahertz to tens of gigahertz [7], which is a bottleneck of the electronic technologies.

In general, the items to be measured based on photonics include the frequency, the angle-of-arrival (AOA) and the Doppler frequency shift (DFS). For the measurement of the instantaneous microwave frequency, many approaches based on the frequency-power mapping [8]–[10], Stimulated Brillouin Scattering (SBS) [11] and channelized structure [12] were reported, in which the measurement range is large and tunable and the precision is high. The AOA, as well as the time

difference of arrival (TDOA), can also be detected in the optical domain [13], [14]. The Doppler effect caused by the radial movement between the target and the observer will induce a frequency shift with respect to the wave source which is important in image acquisition, wireless channel estimation and velocity measurement. As for the DFS measurement, the most common electrical approach is the I/Q mixing [15], which can extract the real and imaginary components of the echo signal. However, this method is usually limited by the operating bandwidth. To resolve this problem, many photonics research articles have been published [16]–[20].

In [15] and [16], the authors proposed a standalone Doppler speed estimation system based on Four-wave mixing (FWM) effect. A mapping from the DFS to the amplitude of the low-frequency output signal is established to estimate the signal with carrier frequency up to 40 GHz. However, the accuracy will decrease when operating at high frequency.

Different from the mapping method, the attempts in [17]–[19] exhibit another measurement idea based on the photonic mixing between the transmitted signal and the echo signal. Once the echo signal is down converted, the DFS is subsequently estimated by an electrical spectrum analyzer (ESA). In [17], two external modulators are cascaded and are modulated by the transmitted signal and echo signal, respectively, and then detected by a low-speed photodiode. It is noted that the direction of the DFS cannot be discriminated in this approach; therefore, the scheme is improved in collaboration with a frequency shift module [18]. Hence, the DFS with two signs can be measured but the frequency shift module makes the system bulky. In [19], a 90° optical hybrid and a balanced detector are adopted. In this way, an in-phase (I) and a quadrature (Q) signal are generated and the direction information can be obtained by comparing the phase difference between the waveforms in I and Q branches. The DC component and common-mode noise can be removed by balanced detection.

In this paper, we propose a simple photonic approach for DFS measurement based on a single dual-parallel Mach-Zehnder modulator (DPMZM). In the proposed approach, the transmitted signal and the echo signal are loaded in the upper and lower arm of the DPMZM to perform carrier-suppressed double-sidebands (CS-DSB) modulation respectively. The upper and lower sidebands are separated and then heterodyned respectively. The DFS value can be obtained from the ESA and the phase difference between two branches implies the sign of the DFS. The key significance of the proposed approach is that we can use the phase difference and power of two sidebands to obtain the direction and the absolute value of the DFS simultaneously. In fact, the proposed approach is an equivalent I/Q mixer. The electrical I/Q mixers are now commercially available [20] and working frequency can reach Ka band. However, the working frequency range of the I/Q mixer is limited. Compared with the approaches in [16]–[20], the system is more compact and easy to implement since only one external modulator is used. Experiments are carried out to verify our approach. The measurements at carrier frequency range from 10 GHz to 39 GHz are proved to be effective.

2. Principles

The proposed approach for the DFS measurement is depicted in Fig. 1. A light wave from the laser diode (LD), denoted by $E_{\text{in}}(t)$, is injected into the DPMZM. Two continuous microwave waves which are designated as echo signal and transmitted signal (or LO signal) are applied to the upper and lower MZM to generate the CS-DSB modulation signals. To do so, the two sub-MZMs are biased at null point. The echo signal and transmitted signal are written as $V_E \sin(\omega_E t)$ and $V_T \sin \omega_T t$, where V_E and V_T are the amplitudes, ω_E and ω_T are the angular frequencies respectively. Under the small-signal condition, the output signals from the two sub-MZMs can be approximately written as

$$E_a(t) = \frac{\sqrt{2T}E_{in}(t)J_1(m_E)}{2} \cdot \begin{bmatrix} \exp(j\omega_E t) \\ -\exp(-j\omega_E t) \end{bmatrix} \tag{1}$$

$$E_b(t) = \frac{\sqrt{2T}E_{in}(t)J_1(m_T)}{2} \cdot \begin{bmatrix} \exp(j\omega_T t) \\ -\exp(-j\omega_T t) \end{bmatrix} \tag{2}$$

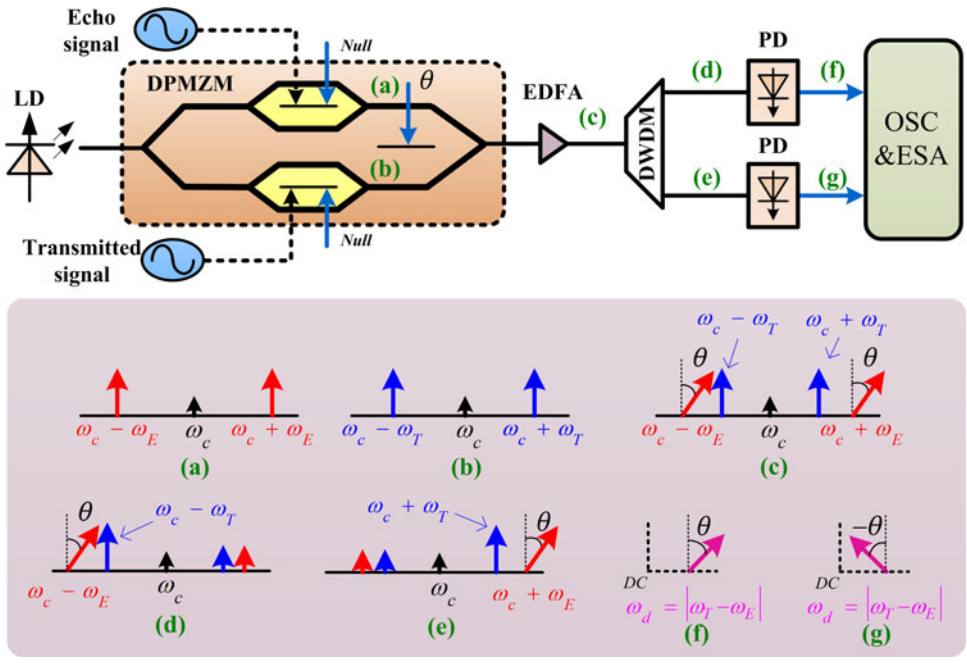

Fig. 1. Schematic diagram of the proposed DFS measurement approach. LD: laser diode; DPMZM: dual-parallel Mach-Zehnder modulator; DWDM, dense wavelength division multiplexer; PD: photodiode; OSC: oscilloscope; ESA: electrical spectrum analyzer. (a)–(e) Schematic optical spectra at specific locations. (f)–(g) Schematic electrical spectrum at specific locations.

where T is the insertion loss of the modulator, and m_E and m_T denote the modulation indexes corresponding to the echo and transmitted signal, respectively. $J_1(\cdot)$ indicates the first order Bessel function of the first kind. As shown in Fig. 1(a) and (b), the CS-DSB signals are produced. The main modulator of the DPMZM is used to introduce a phase difference between two sub-arms, and therefore, the output of the DPMZM can be expressed as

$$E_o(t) = E_a(t) + E_b(t)\exp(j\theta) \tag{3}$$

where $\theta = V\pi/V_\pi$, V, and V_π denote the DC bias and the half-wave voltage of the main-MZM, respectively. The diagrammatic spectrum of $E_o(t)$ is shown in Fig. 1(c). After amplified by an erbium-doped optical fiber amplifier (EDFA), the upper sidebands and lower sidebands are separated with the help of a dense wavelength division multiplexer (DWDM), which are illustrated in Fig. 1(d) and (e). Accordingly, the mathematical expressions can be given by

$$E_{upper} = -\frac{\sqrt{2T}E_{in}(t)}{2}\begin{bmatrix} J_1(m_E)\exp(-j\omega_E t) \\ +J_1(m_T)\exp(-j\omega_T t + j\theta)\end{bmatrix} \tag{4}$$

$$E_{lower} = \frac{\sqrt{2T}E_{in}(t)}{2}\begin{bmatrix} J_1(m_E)\ \exp\ (j\omega_E t) \\ +J_1(m_T)\ \exp\ (j\omega_T t + j\theta)\end{bmatrix}. \tag{5}$$

According to the Doppler effect, we can easily determine the moving direction of the target by discriminating the sign of the subtraction between the echo and transmitted frequency. In more detail, if $\omega_E > \omega_T$, the target is moving towards the observer. Conversely, receding movement will meet the relationship of $\omega_E < \omega_T$. For simplicity, here, we define the DFS as $\omega_d = \omega_E - \omega_T$.

The upper and lower signals are square-law detected by two low-speed photodiodes (PD) since the DFS is usually several kilohertz. Hence, if we tune the θ as $\pi/4$, the obtained electrical fields

can be written as

$$\begin{aligned}\begin{bmatrix} i_u \\ i_l \end{bmatrix} &= T\xi E_0^2 J_1(m_E) J_1(m_T) \begin{bmatrix} \cos[(\omega_E - \omega_T)t + \theta] \\ \cos[(\omega_E - \omega_T)t - \theta] \end{bmatrix} \\ &= T\xi E_0^2 J_1(m_E) J_1(m_T) \begin{cases} \begin{bmatrix} \cos(|\omega_d| t + \pi/4) \\ \cos(|\omega_d| t - \pi/4) \end{bmatrix} & \omega_E > \omega_T \\ \begin{bmatrix} \cos(|\omega_d| t - \pi/4) \\ \cos(|\omega_d| t + \pi/4) \end{bmatrix} & \omega_E < \omega_T \end{cases} \end{aligned} \tag{6}$$

where ξ represents the response of the PD. E_0 is the amplitude of the optical carrier from the LD.

As can be seen from (6), we can acquire absolute value of the DFS by analyzing the electrical signal in either upper or lower channel. The sign of the DFS can be differentiated by comparing the phase difference of the upper and lower branches. If the upper branch is $\pi/2$ advanced with respect to that of the lower branch, a positive DFS is acquired. Otherwise, a negative DFS can be obtained when the upper branch is $\pi/2$ delayed.

In practical situations, the echo signals are usually phase delayed and can be expressed as $V_E \sin(\omega_E t + \varphi)$. Then, the obtained electrical fields can be written as follows:

$$\begin{bmatrix} i_u \\ i_l \end{bmatrix} = T\xi E_0^2 J_1(m_E) J_1(m_T) \begin{cases} \begin{bmatrix} \cos(|\omega_d| t + \pi/4 + \varphi) \\ \cos(|\omega_d| t - \pi/4 + \varphi) \end{bmatrix} & \omega_E > \omega_T \\ \begin{bmatrix} \cos(|\omega_d| t - \pi/4 - \varphi) \\ \cos(|\omega_d| t + \pi/4 - \varphi) \end{bmatrix} & \omega_E < \omega_T. \end{cases} \tag{7}$$

Equation (7) indicates that the direction of the DFS can be still distinguished even if the echo signal has a phase difference with respect to the transmitted signal because the two down-converted signals in upper and lower branches are simultaneously φ delayed or advanced. Moreover, the approach is independent of the transmitted carrier frequency, ensuring a wide operation band.

3. Experiments and Discussion

3.1 Experiment Setup

The experiment system of the proposed DFS measurement scheme is set up based on Fig. 1. A continuous light wave with a power of 15 dBm and wavelength around 1552 nm is generated from a distributed feedback LD (Emcore, 1782). Since the pigtail of the LD is polarization-maintaining, the light is directly injected into the DPMZM (FTM7961, half-wave voltage 3.5 V) without any polarization control. The echo signal with a power of 0 dBm generated from a vector signal generator (VSA, Rohde & Schwarz, SMW200A, 40 GHz) is applied to the upper arm of the DPMZM. Similarly, the lower arm is loaded by the 10 dBm transmitted signal generated from a microwave signal generator (MSG, Agilent, N5183A MXG). Both arms are biased at null point. Then the output of the DPMZM is amplified to 15 dBm by an EDFA. Then, a flat-top arrayed waveguide grating (AWG) DWDM with 50 GHz spacing is utilized to separate upper and lower sidebands. Two adjacent channels around 1552 nm are used. After being filtered by the DWDM, the optical signals in two channels are, respectively, detected by two PDs with a bandwidth of 1 GHz and responsivity of 0.88 A/W. Finally, the electrical signals are monitored by the ESA (Rohde & Schwarz, FSW50) and an OSC (Tektronix DPO7254, 2.5 GHz bandwidth, 40 GS/s).

First of all, to show that the system is capable of simultaneously measuring the absolute value as well as the sign of the DFS, the transmitted signal is set to be 20 GHz and the echo signal has a frequency of 20.001 GHz (or 19.999 GHz) to form a DFS of +1 MHz (or –1 MHz). The CS-DSB modulated signals with a carrier suppression ratio of 33.3 dB are shown in Fig. 2(a).The responses of the DWDM are also plotted. Since the resolution of our spectrograph (Advantest

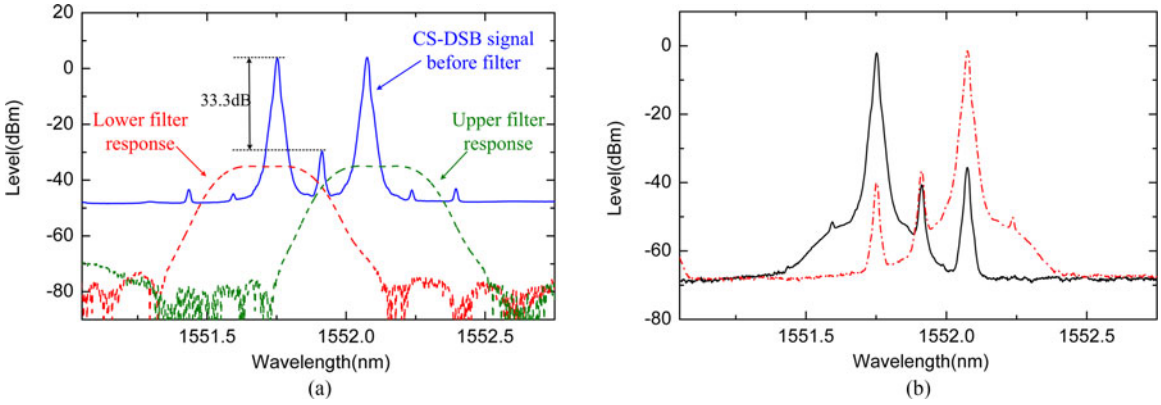

Fig. 2. Measured (a) CS-DSB modulation signals before filter and frequency responses of two adjacent DWDM channels. (b) Upper sidebands and lower sidebands after filter.

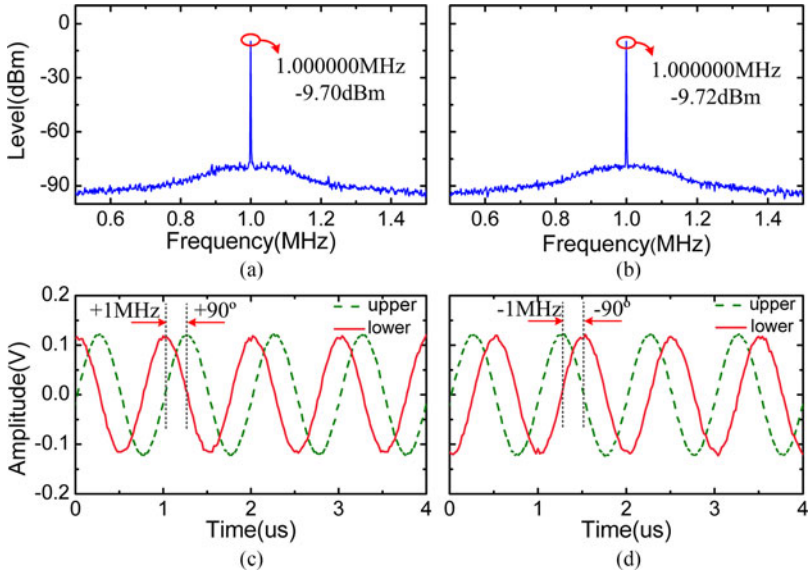

Fig. 3. Measured electrical spectra of upper channel for the DFS at (a) +1 MHz and (b) –1 MHz, and the waveforms of the upper and lower channels for the DFS at (c) +1 MHz and (d) –1 MHz.

Q8384) is 0.01 nm, the transmitted and echo components cannot be resolved. After filtering, the upper sidebands and lower sidebands are separated thoroughly, as shown in Fig. 2(b).

The separated optical signals are respectively injected to the PDs. When the echo signal is at 20.001 GHz (+1 MHz DFS), the measured electrical spectrum of the upper channel is shown in Fig. 3(a). It is clearly seen that only the signal with absolute frequency value of the DFS is obtained with a high signal-to-noise ratio. Thanks to the high resolution of the ESA, the accurate value of the DFS can be read out from the screen. The waveforms of the two channels are captured by the OSC. Here, we adjust θ to be 45°. A phase difference of 90° between the upper and lower channel can be obtained theoretically. As can be seen from Fig. 3(c), the signal in the upper branch is about 90° advanced with respect to that of the lower branch, which is consistent with the theory. Likewise, Fig. 3(b) and (d) illustrate the electrical spectrum and waveforms when the echo signal is at 19.999 GHz (–1 MHz DFS), we can see that the DFS is measured precisely as well, and the sign is discriminated clearly.

Then we test different DFS values at 20 GHz by tuning the echo signal from 19.9999 GHz to 20.0001 GHz with a step of 10 kHz, indicating the DFS varies from –100 kHz to + 100 kHz. The

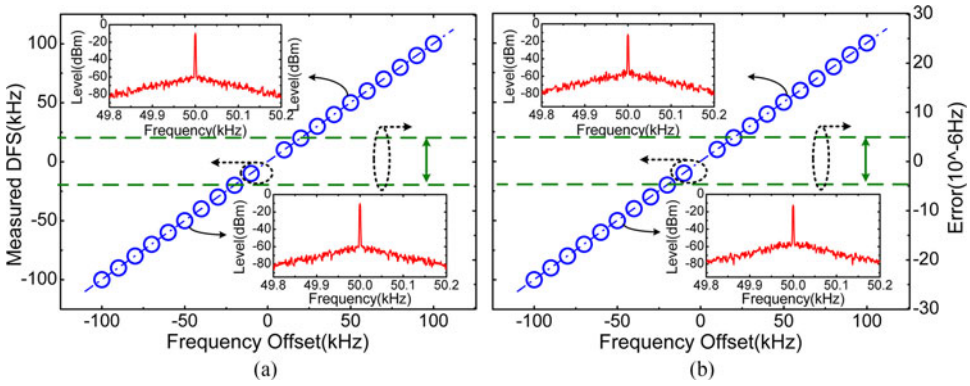

Fig. 4. Measured Doppler frequency shifts from –100 kHz to + 100 kHz, frequency spectra at ±50 kHz, and corresponding error boundaries at the carrier frequencies of (a) 20 GHz and (b) 39 GHz.

ESA is tuned manually to have a span of 2 kHz, resolution bandwidth of 10 Hz and video bandwidth of 10 Hz. In Fig. 4(a), the measured frequencies plotted as circles are extremely close to the theoretical frequency offsets. To clearly illustrate the measurement results, the frequency spectra at the DFS of +50 kHz and –50 kHz are shown by the insets in Fig. 4(a). It is particular to note that the DFS of zero frequency is not demonstrated since we cannot extract the DFS from large DC component.

In our experimental demonstration, the DFS is simulated by two continuous wave sources with a slight frequency shift. By comparing the measured frequencies with the frequency offsets, we can get the measured error. As shown in Fig. 4(a), the resultant errors of the DFS at 20 GHz are lower than 5×10^{-6} Hz which is given by a maximum boundary value marked in dotted line. The errors mainly rest on the performance of the ESA, and fortunately, FSW50 has an extremely high resolution at low frequency range. Lower errors can be obtained if an ESA with better performance is available. It is noted that the two microwave signals are synchronized to cancel their frequency instability and reduce the errors.

In order to investigate that the proposed system can be performed at a wide carrier frequency range. The frequency of the transmitted signal is reset as 39 GHz in our experiment. Similarly, the measured DFS, frequency spectra and measured errors at different carrier frequencies are accordingly plotted in Fig. 4(b), respectively. We can see that the value as well as the sign is well estimated. The insets in Fig. 4(b) give different frequency spectra, while the peak frequencies are exactly the same. That is the reason that similar errors are observed. In fact, 10-GHz and 30-GHz carrier frequencies are also verified in our experiment, similar results can be obtained. Since the MSG and the VSA used have bandwidth of 40 GHz, higher carrier frequency cannot be demonstrated. In fact, the carrier frequency tunable range is restricted by the optical filter. If a band-pass filter with a larger passband is available, the higher carrier frequency can be performed. In addition, a steeper stopband attenuation of the filter will also increase the tunable range.

3.2 Discussion

Considering that the echo signal is usually mingled in noise, the effect of the noise on the system is discussed. Assuming that an additive white noise is embedded into the echo signal, the echo signal can be re-expressed as $V_E \sin(\omega_E t) + n(t)$. The noises from the optical link would also deteriorate the signal-to-noise ratio (SNR) of the system. At the output of the PD, the SNR can be written as

$$\text{SNR} = \frac{G P_{signal}}{G N_{in} + N_{ASE} + N_{RIN} + N_{shot} + N_{thermal}}. \quad (8)$$

Here, P_{signal} is the power of the echo signal; G is the gain of the system; N_{in} is the input additive noise; N_{ASE} is the signal-spontaneous beat noise from the EDFA; and N_{RIN}, N_{shot}, and $N_{thermal}$ are

TABLE 1
Measured and Theoretical SNRs

Input SNRs (dB)	Measured noise (dBm/Hz)	Measured signal power (dBm)	Measured SNRs (dB)	Theoretical SNRs (dB)
20	–100.11	–27.92	19.18	19.9
10	–90.23	–27.90	9.32	9.9
0	–80.51	–27.84	-0.34	0

the laser RIN noise, the shot noise, and the thermal noise, respectively [22]. The noises generated from the optical link can be given by

$$\begin{aligned} N_{ASE} &= hvn_{sp}\xi P_{pd}\left(G_{EDFA}-1\right)R_L B_e \\ N_{RIN} &= 10^{RIN/10}\left(\xi P_{pd}\right)^2 R_L B_e/4 \\ N_{shot} &= q\xi P_{pd} R_L B_e/2 \\ N_{thermal} &= (1+G)\,kTB_e \end{aligned} \tag{9}$$

where h is the Planck constant (6.62607 $\times$ 10ˆ-34 J·s), v is the optical frequency, n_{sp} is the spontaneous emission factor, P_{pd} is input optical power of the PD, G_{EDFA} is the gain of the EDFA on linear scale, R_L is the detector impedance (50 Ω), q is the fundamental charge (1.6021892 $\times$ 10ˆ-19 C), RIN is the laser relative intensity noise [-155 dB/Hz], k is Boltzmann's constant (1.3806505(24) $\times$ 10ˆ-23 J/K), T is room temperature (290 K), and B_e is the noise bandwidth. G is the gain of the system on linear scale.

An experiment is carried out to measure the SNR. Here, we set the power of the echo signal as –20 dBm, noise bandwidth as 200 kHz, the gain of the EDFA as 30 dB. The measured gain of the system is –7.9 dB, P_{pd} is 5.6 dBm. The calculated value of N_{ASE}, N_{RIN}, N_{shot} and $N_{thermal}$ are –130.4, –164.0, –169.0 and -173.3 dBm/Hz, respectively. Note that the noises generated from the optical link are much lower than the additive noise, the SNR of the echo signal will not be deteriorated a lot by the system. Different SNRs (i.e., 20, 10, 0 dB) can be obtained by changing the power of the additive noise. The corresponding experimental results are depicted in Table 1. The calculated theoretical results are also given according to (8) under the same conditions. As illustrated in Table 1, the measured SNRs of the down-converted electrical signal are 19.18, 9.32 and –0.34 dB, respectively, which are close to the input SNRs. The measured results accord well with theoretical values.

4. Conclusion

In conclusion, a simple photonic approach for DFS measurement based on a single DPMZM is proposed and experimentally demonstrated. The phase relationship and the power of two CS-DSB sidebands are fully employed to measure the DFS absolute values and discriminate the directions. A wide carrier frequency range from 10 GHz to 39 GHz is achieved with measurement errors within 5×10^{-6} Hz. If a DWDM with wider passband and larger FSR is available in our lab, the range can be further enlarged. The system is compact and easy to implement, which provides an alternative approach to realize the measurement of the DFS.

References

[1] J. Yao, "Microwave photonics," *J. Lightw. Technol.*, vol. 27, no. 3, pp. 314–225, Feb. 2009.
[2] J. D. Mckinney, "Technology: Photonics illuminates the future of radar," *Nature*, vol. 507, no. 7492, pp. 310–311, Mar. 2014.
[3] P. Ghelfi *et al.*, "A fully photonics-based coherent radar system," *Nature*, vol. 507, no. 7492, pp. 341–345, Mar. 2014.
[4] J. Xiao *et al.*, "W-band OFDM photonic vector signal generation employing a single Mach–Zehnder modulator and precoding," *Opt. Exp.*, vol. 23, no. 18, pp. 24029–24034, Sep. 2015.
[5] F. Laghezza, F. Scotti, P. Ghelfi, and A. Bogoni, "Photonics-assisted multiband RF transceiver for wireless communications," *J. Lightw. Technol.*, vol. 32, no. 16, pp. 2896–2904, Aug. 2014.
[6] S. Pan *et al.*, "Satellite payloads pay off," *IEEE Microw. Mag.*, vol. 16, no. 8, pp. 61–73, Sep. 2015.
[7] X. Zou, B. Lu, W. Pan, L. Yan, A. Stohr, and J. Yao, "Photonics for microwave measurements," *Laser Photon. Rev.*, vol. 10, pp. 1–24, 2016.
[8] X. Li *et al.*, "Photonic microwave frequency measurement with a tunable range based on a dual-polarization modulator," *OSA Appl. Opt.*, vol. 55, no. 31, pp. 8727–8731, Nov. 2016.
[9] X. Zou and J. Yao, "An optical approach to microwave frequency measurement with adjustable measurement range and resolution," *IEEE Photon. Technol.* vol. 20, no. 23, pp. 1989–1991, Dec. 2008.
[10] H. Zhang and S. Pan, "High resolution microwave frequency measurement using a dual-parallel mach–zehnder modulator," *IEEE Microw. Wireless Compon. Lett.*, vol. 23, no. 11, pp. 623–625, Nov. 2013.
[11] S. Zheng, S. Ge, X. Zhang, H. Chi, and X. Jin, "High-resolution multiple microwave frequency measurement based on stimulated brillouin scattering," *IEEE Photon. Technol. Lett.*, vol. 24, no. 13, pp. 1115–1117, Jul. 2012.
[12] H. Chen *et al.*, "Photonics-assisted serial channelized radio-frequency measurement system with Nyquist-bandwidth detection," *IEEE Photon. J.*, vol. 6, no. 6, Dec. 2014, Art. no. 7903707.
[13] Z. Cao *et al.*, "Phase modulation parallel optical delay detector for microwave angle-of-arrival measurement with accuracy monitored," *Opt. Lett.*, vol. 39, no. 6, pp. 1497–1500, Mar. 2014.
[14] X. Zou *et al.*, "Photonic approach to the measurement of time-difference-of-arrival and angle-of-arrival of a microwave signal," *Opt. Lett.*, vol. 37, no. 4, pp. 755–757, Feb. 2012.
[15] V. C. Chen, "The micro-Doppler effect in radar: phenomenon, model, and simulation study," *IEEE Trans. Aerosp. Electron. Syst.*, vol. 42, no. 1, pp. 2–21, Mar. 2006.
[16] H. Emami, M. Hajihashemi, and S. Alavi, "Standalone microwave photonics Doppler shift estimation system," *J. Lightw. Technol.*, vol. 14, no. 8, pp. 3596–3602, Aug. 2016.
[17] H. Emami, M. Hajihashemi, and S. Alavi, "Improved sensitivity RF photonics doppler frequency measurement system," *IEEE Photon. J.*, vol. 8, no. 5, Oct. 2016, Art. no. 5501308.
[18] X. Zou, W. Li, B. Lu, W. Pan, L. Yan, and L. Shao, "Photonic approach to wide-frequency-range high-resolution microwave/millimeter-wave Doppler frequency shift estimation," *IEEE Trans. Microw. Theory Techn.*, vol. 63, no. 4, pp. 1421–1430, Apr. 2015.
[19] B. Lu *et al.*, "Wideband Doppler frequency shift measurement and direction ambiguity resolution using optical frequency shift and optical heterodyning," *OSA Opt. Lett.*, vol. 40, no. 10, pp. 2321–2324, May 2015.
[20] B. Lu *et al.*, "Wideband microwave Doppler frequency shift measurement and direction discrimination using photonic I/Q detection," *J. Lightw. Technol.* vol. 34, no. 20, pp. 4639–4645, Oct. 2016.
[21] Internet site. [Online]. Available: http://www.markimicrowave.com/ IQ-Mixers-View-All-C143.aspx
[22] C. Middleton, M. Borbath, and J. R. DeSalvo, "Measurement of SFDR and noise in EDF amplified analog RF links using all-optical down-conversion and balanced receivers," in *Proc. Conf. Enabling Photon. Technol. Defense, Security, Aerosp. Appl. IV*, 2008, pp. 69750Q-1–69750Q-12.